Calibrating a Solar X-Ray Detector Using Radioactive Sources with Discrete Spectra

By Jamison Ward

ward0975@umn.edu

Introduction & Background

Calibrating a solar x-ray detector is critical to permit the accurate scientific investigation of solar flares and coronal mass ejections (CMEs). These cataclysmic solar phenomena pose risks to life and modern technology on and orbiting the Earth by causing geomagnetic storms upon collision with the Earth's magnetosphere.[1] Investigating the underlying causes of these solar phenomena would improve the ability to forecast such events and understand their impact on Earth's various electrical and communication systems.[2]

One method of studying the mechanisms that produce solar flares and CMEs is by observing the radiation associated with these events using small satellites called CubeSats. The Impulsive Phase Rapid Energetic Solar Spectrometer (IMPRESS) satellite is a University of Minnesota Small Satellite Research Laboratory (UMN SSRL) project in collaboration with Montana State University, UC Santa Cruz, and the Southwest Research Institute and is funded by the National Science Foundation. The IMPRESS satellite contains two sets of on-board detectors designed to observe x-ray photons produced in conjunction with solar flares and CMEs in different energy bands: the X-123 semiconductor detector (4-12 keV) and the HaFX scintillator detector (8-100 keV).

This project concerns the main detector on IMPRESS, the Hard and Fast X-ray spectrometer (HaFX), which is a scintillation-based x-ray spectrometer that converts incident photons into electrical signals using a silicon photomultiplier (SiPM). These signals are then converted into voltage pulses that are digitized and sorted into a histogram stored in the satellite's memory.[3] Thus, each bin in the digital histogram theoretically corresponds to a specific incident photon energy. To ensure that the data transmitted from the IMPRESS satellite is reliable, the relationship between histogram bin number and incident photon energy must be known.

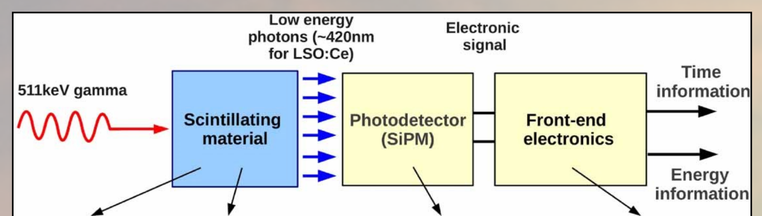

Figure 1: *A schematic of a scintillator detector that uses a silicon photomultiplier. The electrical signal produced by the scintillation crystal is amplified by the SiPM, producing a voltage pulse that is digitized and recorded by the detector in a histogram. Stefan Gundacker and Arjan Heering 2020 Phys. Med. Biol.* ***65*** *17TR01. Figure 18. https://iopscience.iop.org/article/10.1088/1361-6560/ab7b2d#pmbab7b2deqn15*

Experiment & Analysis

Throughout this experiment, a prototype scintillation detector called the SiPM-3000 served as a testing analog to HaFX, which uses the same silicon photomultiplier as the SiPM-3000.

To simulate the range of photon energies the satellite will record while in orbit, multiple radioactive sources with known emission lines in the x-ray band (~1-100 keV) were observed by the SiPM-3000 to characterize the detector's behavior at these energies. The utilized sources included Americium-241, Barium-133, Bismuth-207, and Cesium-137. Since radioactive decay is a fundamentally random process,[4] data from each source were collected for 5 minutes, producing spectra with enough counts to clearly distinguish each peak for analysis.

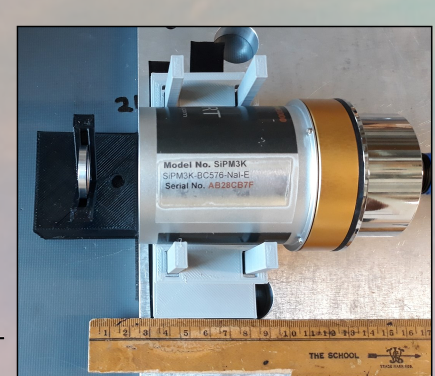

Figure 2: *SiPM-3000 in testing configuration with Am-241 source.*

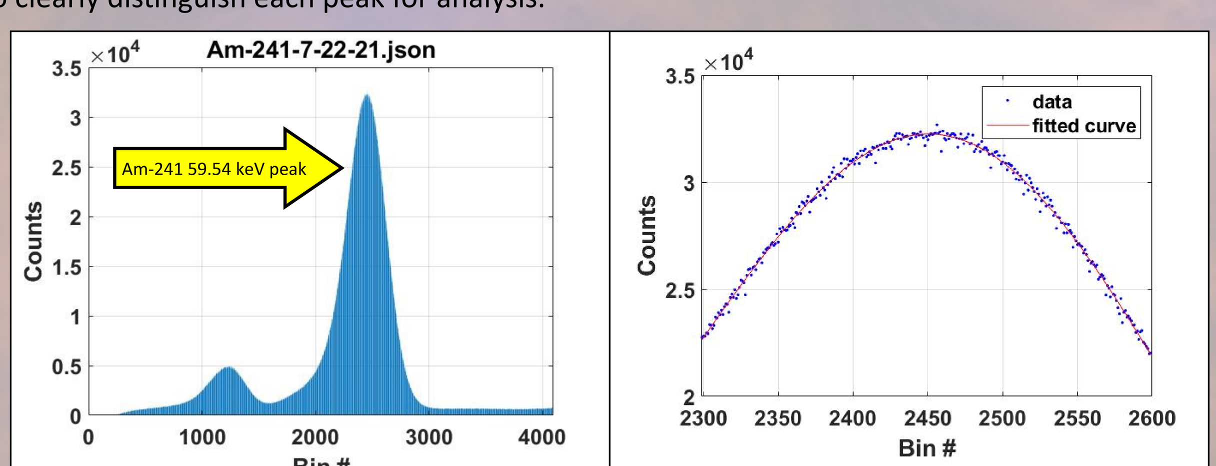

Figure 3: *An observed spectrum of Am-241 as a histogram (left) and a Gaussian fit applied to the characteristic 59.54 keV peak (right).*

Using a MATLAB program provided by the UMN SSRL detector team, a Gaussian distribution function was fit to each peak multiple times over a series of ranges that incremented outward and inward by 50-bin intervals from the peak's full-width half-maximum bounds, not exceeding an expansion/contraction of 200 bins. The average of these results was taken as the bin corresponding to the spectral peak.

In the case that a histogram peak was comprised of photons from multiple source emission lines, a Python program written by this project's author was utilized to assign an appropriate energy to each peak. This program first applied a multiplier to each line's relative intensity[5] to account for the photon flux attenuation caused by the detector's aluminum housing[6] and then performed a weighted average of the coincident emission line energies based on their adjusted relative intensities.

Results & Error

The resulting peak bin numbers were plotted against the corresponding weighted emission line energies in figure 4. A linear trend is observed in the data with a slight tapering occurring on the high energy end of the data range. A line of best fit was calculated for this data set by minimizing the chi-squared value for the y-intercept and slope parameters, which is defined as

$$\chi^2 = \sum_i^n \frac{[y_i - (a + bx_i)]^2}{\sigma_i^2} \qquad (1)$$

where a is the y-intercept parameter, b is the slope parameter, and σ is the error in the y variable (bin number). This method was utilized because the relative uncertainty in the emission line energies was much lower than the relative uncertainty in the peak bin numbers as shown in table 1. Performing this linear fit yielded a slope parameter of 40.45 ± 0.06 bins/keV and a y-intercept parameter of 12.57 ± 4.54 bins.

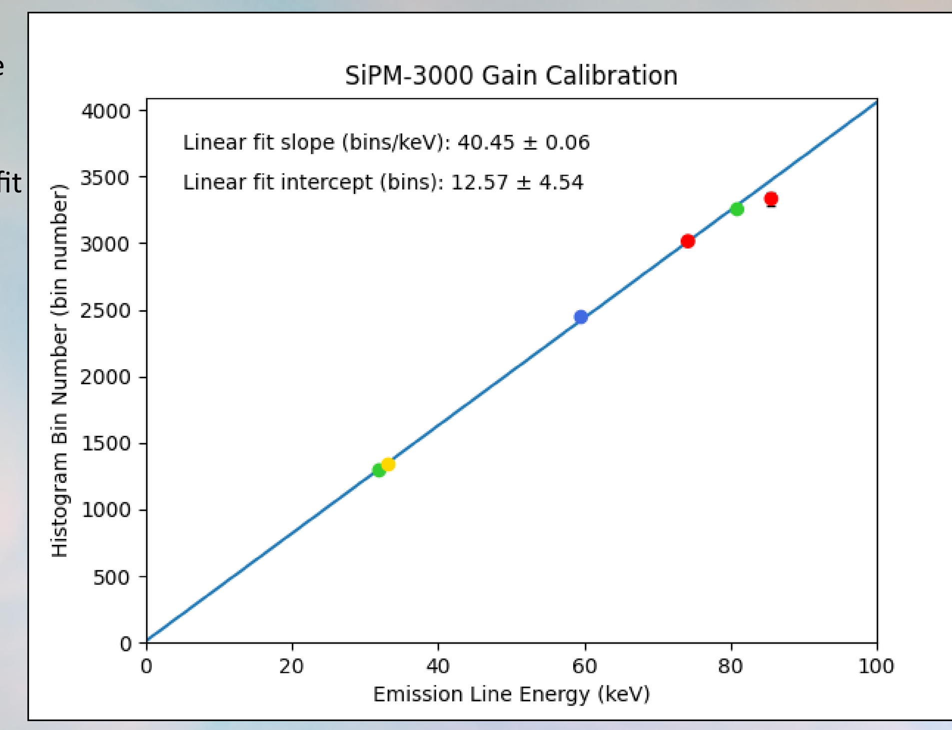

Figure 4: *A plot of the peak histogram bin numbers versus the radiation source emission line energies. All error bars except for the those of the upper right, red*

The error in the peak bin location was calculated by finding the standard deviation in the series of bin measurements obtained from the Gaussian fits described in the experiment & analysis section. The error on the 85.56 keV Bi-207 peak is abnormally large because this peak was contained within the primary 74.17 keV Bi-207 peak as depicted in figure 5. Resolving both peaks required the use of a two-term Gaussian function, leading to a higher uncertainty in the location of the secondary 85.56 keV peak in the histogram.

Source	Peak Energy (keV)	Energy Error (keV)	Avg. Peak Bin	Bin Error
Americium-241	59.5412	0.0001	2446	3
Barium-133	31.915	0.008	1294	3
	80.897	0.007	3255	3
Bismuth-207	74.167	0.015	3015	1
	85.563	0.018	3334	50
Cesium-137	33.161	0.008	1338	6

Table 1: *A summary of the calculated weighted emission line energies and the corresponding peak bin numbers obtained from the experiment.*

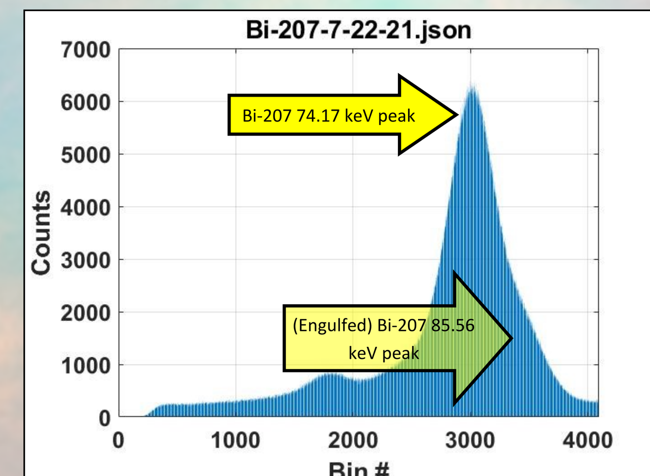

Figure 5: *The two Bi-207 lines are not distinct and thus required a two-term Gaussian to resolve. The less intense 85.56 keV peak appears as a shoulder on the main 74.17 keV peak.*

The error in the emission line energy was found by first propagating the exponential attenuation law (equation 2) with respect to the incident photon flux intensity (I_0) and the thickness of the detector's aluminum housing (t) to determine the error in intensity adjusted for attenuation. In equation 2, μ/ρ is the mass attenuation coefficient, ρ is the density of the attenuating material, and $x = \rho t$ is the mass thickness. The errors associated with the mass attenuation coefficient and aluminum density values were negligible.

$$I = I_0 e^{-(\mu/\rho)x} \qquad (2)$$

With the adjusted intensity uncertainty calculated for each emission line, the error in the final weighted energy was propagated with respect to the adjusted intensity (I_i) of each line in the weighted average formula (equation 3). Additionally, the error associated with each emission line energy (E_i) was also negligible.

$$E_f = \frac{\sum_i^n E_i I_i}{\sum_i^n I_i} \qquad (3)$$

Finally, the uncertainty in the y-intercept (σ_a) and slope (σ_b) parameters in the fit line were determined from the chi-squared formalism described above. Specifically, these values were obtained from the following set of equations.

$$\sigma_a{}^2 = \frac{1}{\Delta}\sum_i^n \frac{x_i{}^2}{\sigma_i{}^2} \qquad \sigma_b{}^2 = \frac{1}{\Delta}\sum_i^n \frac{1}{\sigma_i{}^2} \qquad \Delta = \sum_i^n \frac{x_i{}^2}{\sigma_i{}^2}\sum_i^n \frac{1}{\sigma_i{}^2} - \left[\sum_i^n \frac{x_i}{\sigma_i{}^2}\right]^2$$

Bibliography

[1] Falewicz, R. (2014). *Plasma heating in solar flares and their soft and hard X-ray emissions.* The Astrophysical Journal, 789(1), 71.

[2] Holman, Gordon D. (2012). *Solar eruptive events*. Physics Today, 65(4), 56-61.

[3] Erickson, K. (2019) *Characterization of gain and low energy threshold of cesium iodide thallium doped incident energy spectrometer* [UMN astrophysics senior thesis]. University of Minnesota, Twin Cities.

[4] Redus, R. (2018, January 18). *Fundamentals of radiation detection & measurement*. 2017 IEEE Nuclear Science Symposium, Atlanta, Georgia.

[5] Be, M.-M., Chiste, V., Dulieu, C., Kellett, M. A., Mougeot, X., Arinc, A., Chechev, V. P., Kuzmenko, N. K., Kibedi, T., Luca, A., & Nichols, A. L. (2016). Table of Radionuclides (Vol. 8 - A = 41 to 198). Gif-sur-Yvette, France. http://www.lnhb.fr/nuclear-data/nuclear-data-table/.

[6] Hubbell, J. H., & Seltzer, S. M. (2004, July). X-Ray Mass Attenuation Coefficients. https://dx.doi.org/10.18434/T4D01F.

Poster Background: NASA/JPL-Caltech/GSFC Photojournal: PIA18906. https://photojournal.jpl.nasa.gov/catalog/PIA18906

Conclusion

The study of energetic solar phenomena such as solar flares and coronal mass ejections requires the use of highly accurate and sophisticated equipment in order to obtain scientifically usable data. One component critical to the success of the IMPRESS CubeSat is the calibration of the satellite's detectors, specifically gain calibration, which concerns the ability of IMPRESS to accurately detect and record incident photon energies.

The SiPM-3000 is a scintillation-based x-ray spectrometer that served as a testing analog to the scintillation detector that will fly on IMPRESS. The SiPM-3000 records and sorts incident photons into a digital histogram based on their energies. The relationship between histogram bin number and incident photon energy was quantified by examining a series of radioactive sources with known emission line energies in the x-ray band (~1-100 keV).

Plotting the histogram bin number of each radioactive source's spectral peaks against their corresponding emission line energies yielded a roughly linear correlation between histogram bin number and incident photon energy with the possibility of a nonlinearity on the high energy end of the source data. However, given that the majority of the data are linear, this relation was modeled with a linear regression using the method of minimizing chi-squares to calculate the y-intercept (a) and slope (b) parameters for an equation of the form

$$y = a + bx \qquad (4)$$

The values of these parameters were $a = 12.57 \pm 4.54$ bins and $b = 40.45 \pm 0.06$ bins/keV.

By solving equation 4 for the x variable, the slope of the gain calibration (figure 4) can be expressed in terms of keV/bin. Doing so yields a slope of 0.02472 ± 0.00004 keV/bin and an offset of -0.3108 ± 0.1122 keV; alternatively, these values are 24.72 ± 0.04 eV/bin and -310.8 ± 112.2 eV. Expressing the parameters in this way clarifies the energy distinction between bins in the digital histogram. In the future, a similar calibration procedure will be performed with the detector that will fly on the IMPRESS satellite.

Future Plans

To more accurately assess the performance of the SiPM-3000 over all energies in the x-ray band, particularly at low energies (< 20 keV) and high energies (80-100 keV), the detector will be tested in conjunction with the Amptek Mini-X2 x-ray tube source and possibly other radionuclides with different emission line energies than those used in this gain calibration. Specifically, the x-ray generator contains a tungsten target material that will produce a few characteristic lines. Any new lines observed by the SiPM-3000 will prove instrumental in further characterizing the relationship between histogram bin number and incident photon energy and resolving any nonlinearities that may be present at the extremes of the 1-100 keV energy band. The x-ray generator will arrive at the University of Minnesota Small Satellite Research Laboratory sometime during September of 2021 and should be operational shortly thereafter.

The lower energy peak observed in the Am-241 spectrum (figure 3) was not included in the gain calibration; this peak is a combination of characteristic lines from multiple sources and requires more sophisticated analysis. Firstly, Am-241 has several x-ray and gamma emissions in the 20-30 keV range. Additionally, ionization of the scintillator crystal's iodine atoms by an incident Am-241 59.54 keV photon sometimes results in the escape of the secondary x-ray emitted by iodine from the detector. Consequently, the resulting scintillation event will produce a lower observed energy since the secondary photon failed to ionize additional iodine atoms. The energy of these secondary x-rays ranges from 28-33 keV, meaning the scintillation event triggered by a 59.54 keV photon will occasionally register an energy of only roughly 26-32 keV, which is coincident with the lower energy Am-241 lines described above.

A testing plan to resolve this issue will be created by the UMN Small Satellite Research Laboratory detector team over the course of the fall 2021 semester. This plan will likely include methods to evaluate the relative intensities of the lower energy Am-241 lines and the reduced-energy 59.54 keV photons so that an appropriate energy can be assigned to the Am-241 peak in question using the weighted averaging technique detailed in the experiment & analysis section.

Acknowledgments

UMN Office of Undergraduate Research - Undergraduate Research Opportunities Program

UMN Small Satellite Research Laboratory

Lindsay Glesener - IMPRESS lead project scientist, UROP advisor

William Setterberg - IMPRESS project scientist

Lestat Clemmer - Detector team lead

Ben Willis - Former detector team lead

University of Minnesota
Driven to Discover